IEEE Access
Multidisciplinary | Rapid Review | Open Access Journal

Received April 29, 2021, accepted May 4, 2021, date of publication June 23, 2021, date of current version July 13, 2021.

Digital Object Identifier 10.1109/ACCESS.2021.3078028

Nonparametric Model-Based Online Junction Temperature and State-of-Health Estimation for Insulated Gate Bipolar Transistors

XIANGXIANG LIU[1], TIANLEI JIAO[2], DIGANTA DAS[3], (Member, IEEE), IJAZ HAIDER NAQVI[4], (Member, IEEE), AND MICHAEL PECHT[3], (Life Fellow, IEEE)

[1]State Key Laboratory of Reliability and Intelligence of Electrical Equipment, Hebei University of Technology, Tianjin 300000, China
[2]Beiyang Hongyun (Tianjin) Cyber Technology Ltd., Tianjin 300000, China
[3]Center for Advanced Life Cycle Engineering (CALCE), University of Maryland, College Park, MD 20742, USA
[4]Department of Electrical Engineering, Lahore University of Management Sciences (LUMS), Lahore 54792, Pakistan

Corresponding author: Tianlei Jiao (tianleijiao@gmail.com)

This work was supported by the Joint Doctoral Training Foundation of Hebei University of Technology (HEBUT).

ABSTRACT Insulated gate bipolar transistor (IGBT) is widely used in power equipment, it generally works in complex circuit profiles and it is very difficult to measure or predict the thermal parameters of the module in real-time and evaluate the corresponding health status in the transient process. This paper develops a novel approach for solder-layer condition monitoring of IGBTs. In the approach a time-series nonparametric model of a power module is constructed, the current power and ambient temperature data are used to deduce the health state junction and case temperature. Three groups of time-series insulated gate bipolar transistors (IGBTs) data are used to train and verify the time-series nonparametric model for online conditions, the results show that the developed method has high accuracy. Compared with traditional methods, the time series non-parametric model method not only saves characteristic experiments but also saves the process of mathematical model construction. Besides, the proposed method also has the advantages of strong generalization and low equipment requirements which is useful for actual working conditions. Thereafter, another nonparametric model is built, the predicted junction temperature is used to estimate the collector voltage in the health state, and the percentage deviation of the measured collector voltage from the estimated voltage is used to do the state-of-health estimation of the IGBT and its accuracy is verified by the experiment result.

INDEX TERMS IGBT, time-series ANN, state-of-health, junction temperature, artificial intelligence.

I. INTRODUCTION

Power inverters are one of the most reliability-critical parts in power electronic systems such as photovoltaic (PV) systems and wind-power generation systems. For example, an investigation of wind turbines showed that the power electronic frequency converters caused 13% of the failures and 18.4% of the downtime of the monitored wind turbines [1]. Insulated-gate bipolar transistors (IGBTs) are estimated to be responsible for 34% of all inverter failures, indicating that the reliability of power electronics is highly correlated with the reliability of the IGBT module [2], [3]. Improved diagnostics and prognostics of the IGBT module can significantly reduce the downtime and the operational cost of overall PV and wind power generation systems.

Wear-out is the most dominant failure mechanism of power semiconductor devices and the main reason for that is thermo-mechanical stress caused by junction temperature fluctuation [4]. Online junction temperature estimation leads to the state of health estimation. There are a few methods for measuring and estimating the junction temperature. The first method is the optical method which typically uses an infrared (IR) camera. Dupont *et al.* [5] used an IR camera to map the temperature distribution across the chip surface. The main drawback of this method is that the equipment is expensive and not suitable for measurements over a long duration. The second method is the physical attachment method. The attachment materials include thermocouples and optical

The associate editor coordinating the review of this manuscript and approving it for publication was Derek Abbott.

fibers. Piton *et al.* [6] presented an experimental set-up based on optical fibers to measure IGBT chip temperatures online. The drawback of this method is that it destroys the module package, which limits its usage range. The third method is the electrical parameter method. In this method, a temperature-sensitive electrical parameter (TSEP) is used for the junction temperature evaluation. Yuan *et al.* [7] proposed a self-calibration method by using the voltage derivative (dV/dt). Zhang *et al.* [8] used the reverse voltage peak between the auxiliary emitter and power emitter as a TSEP. The advantage of this method is it doesn't need to destroy the package and the accuracy is high by choosing a suitable TSEP. The drawback is that it can only be applied only in low-current situations (usually less than 0.1 A) to avoid self-heating. Some studies established models for online junction temperature estimation. Eleffendi and Johnson [9] estimated online junction temperature by Kalman filter with the auxiliary of collector voltage. Ouhab *et al.* [10] established an analytical electro-thermal model, which can be used during in-service conditions to predict the junction temperature. Junction temperature is critical for the state-of-health estimation of IGBT, but it is general accepted that directly junction temperature is very hard and intrusive It is necessary to do online junction temperature in more effective ways.

Several papers have concentrated on state-of-health estimation and remaining useful lifetime prediction for the online condition. In particular, Hu *et al.* [11] investigated junction and case temperatures at different delamination degrees and an assessment method based on the case temperature difference is established to do the IGBT degradation assessment. The method only works under a stable power or a fundamental frequency power, which might be part of a qualification test. However, the actual working environment of IGBT can be much more complex. Quan *et al.* [12] proposed a multi-label classification learning model based on ISODATA for the multi-feature parameters of power semiconductor device IGBT, the method is proven that it is better at adapting to the IGBT health classification evaluation than general clustering algorithm. Ma *et al.* [13] proposed a health monitoring method by harnessing the inverter operational characteristics and degradation-sensitive electrical parameters to address the IGBT wire bonding faults. The approach obtains both the wire bonding failure features and junction temperature from the terminals of an IGBT module to do online health monitoring. Zhang *et al.* [14] used static and dynamic electrical parameters of IGBT devices as fault precursory the degradation characteristics of on-state voltage drop and the threshold voltage is used for state-of-health estimation. Yang *et al.* [15] proposed an online IGBT junction temperature measurement method based on the on-state voltage drop. It monitors the on-state voltage drop of IGBT and extracts IGBT junction temperature online. Besides, the influences of the measurement circuit temperature variations and IGBT load current variations are compensated based on the off-state stage of the IGBT. The two methods described above note that the on-state collector voltage is highly related to the junction temperature, and the real-time collector voltage can be predicted by the online junction temperature supposing the module is in a healthy state. As a result, using the difference between the predicted value and the measured value, one can assess the state-of-health in real time. Patil *et al.* [16] proposed a prognostic approach by comparing collector voltage before and after degradation. The on-state collector voltage is highly related to the degradation of the module, but the real-time change of the collector voltage before and after degradation still needs to be explored. Ye. *et al.* [17] used the miller platform voltage for online condition monitoring of metal oxide semiconductor field-effect transistors and then predicted the remaining useful lifetime by this parameter. Choi and Blaabjerg [1] studied the effect of junction temperature swing duration and modeled a relevant lifetime factor. Zhang *et al.* [18] proposed a long short-term memory (LSTM) recurrent neural network (RNN) to learn the degradation trajectories of lithium-ion batteries, which is an application of the nonparametric method for lifetime prediction. Although there are relevant research on the state-of-health assessment and key thermal parameters prediction of different devices, the fast thermal response curve prediction and real-time state-of-health estimation of the module still need to be explored.

Machine learning and deep learning are widely used in anomaly detection and automate design, numerous studies have focused on these problems, for example, Zhao *et al.* [19] constructed a deep auto-encoder network to detect early faults in continuously monitored wind turbines. Netam and Yadav [20] proposed non-contact technology for operation-state monitoring based on artificial neural networks (ANN). Li *et al.* [21] applied ANN and K-means clustering for the prediction of IGBT current, then verified that the method can replace the electrical stimulation. Dragicevic *et al.* [22] proposed an automated design of power electronic systems using a nonparametric model. Although a lot of progress has been made, these methods above did not consider time-series parameters for data prediction but which is very valuable. This paper established a time-series nonparametric model under varied conditions to predict the junction temperature and do the state-of-health estimation.

The rest of the paper is organized as follows. Section II presents the overall process flowchart. Section III describes the established process of the thermal simulation model. Section IV presents the process of establishing the time-series nonparametric model and compares the results from the simulation model. Section V shows the online state-of-health estimation prediction process. Section VI presents the conclusions.

II. FLOWCHART OF THE OVERALL PROCESS

As discussed in Section I, it is not easy to obtain the real-time junction temperature during working time. To obtain some real-time data, an accurate simulation model is established in advance. The data is then used for training and testing the time-series nonparametric model.

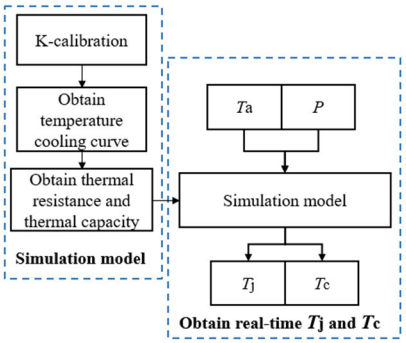

FIGURE 1. Junction and case temperature prediction based on the simulation model.

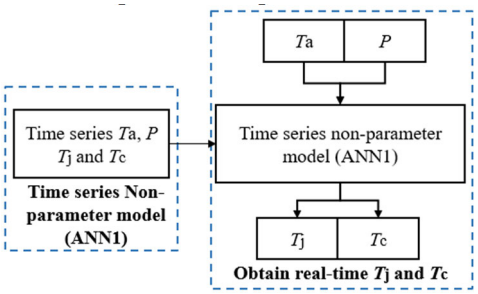

FIGURE 2. Junction and case temperature time-series nonparametric mode.

Figure 1 shows the flowchart to establish a simulation model. In the process, a K calibration coefficient and the temperature cooling curve are required to obtain the thermal resistance and thermal capacitance, which are the main parameters of the thermal simulation model.

Thereafter, a time-series nonparametric model was developed. When establishing the time-series nonparametric model, it requires only a segment of time-series ambient temperature and power. The output is the time-series junction temperature and the case temperature. In figure 2, T_a is the ambient temperature, P is power, T_j is the junction temperature, and T_c is the case temperature. After establishing the time-series nonparametric model, it predicts real-time junction temperature and case temperature by given ambient temperature and power.

The process for training and testing the model is shown in Figure 3. Two different time-series nonparametric models—the artificial neural network (ANN) model and the long short-term memory (LSTM) model—are compared for this specific problem. These two methods show a similar root mean square error (RMSE) of less than 0.3 °C and 0.4 °C respectively. The time-series ANN model was chosen for its higher accuracy. Section IV shows the details of establishing the time-series nonparametric model. The time-series historical data for training and testing the time-series nonparametric model is obtained by the simulation model. The data helps to justify whether the time-series nonparametric model can predict the temperature in different situations when only real-time inputs are given.

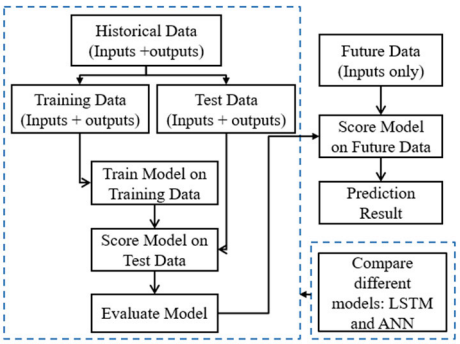

FIGURE 3. Establishing a time-series nonparametric model.

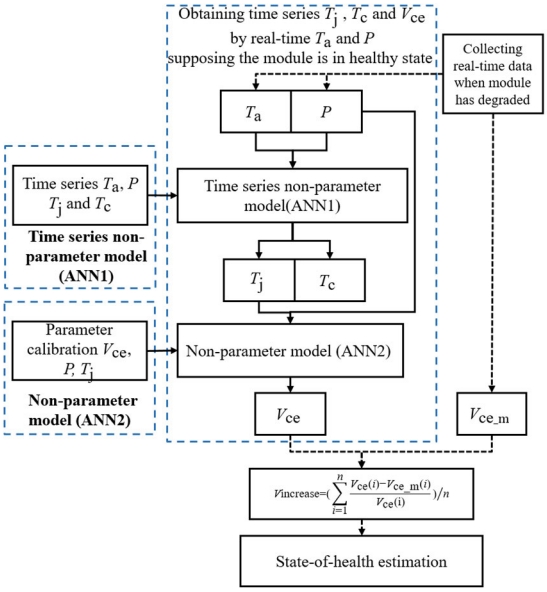

FIGURE 4. State-of-health estimationpredictionby the nonparametric model.

The overall process of predicting temperature and state-of-health estimation is shown in Figure 4. There is a time-series nonparametric model for junction and case temperature prediction and a nonparametric model for collector voltage prediction and state-of-health estimation. The junction temperature, case temperature, and collector voltage under healthy conditions are predicted based on the real-time ambient temperature and power. Therefore, by comparing the measured collector voltage and predicted collector voltage, the mean value of the difference between the measured value (which indicates the degradation state of the module) and the predicted value (which indicates the healthy state of the module) is used to quantify the state-of-health in real-time. Junction temperature is an intermediate variable, the collector voltage in the healthy state is able to deduced under dynamic working conditions and its difference with the measured value is for the state-of-health estimation.

III. THERMAL SIMULATION MODEL

Thermal resistance is a heat property and a measurement of the temperature difference by which an object or material

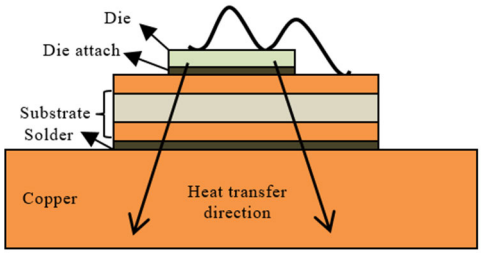

FIGURE 5. IGBT thermal transfer process.

resists a heat flow. The heat transfer process is shown in Figure 5. Thermal resistance is defined in equation 1. T_j is the junction temperature, T_c is the case temperature, and P is power.

$$R_{th} = \frac{T_j - T_c}{P} \tag{1}$$

Thermal capacitance is the ability of the body to store thermal energy, as expressed in equation 2. In the equation, Q is the thermal energy transferred.

$$C_{th} = \frac{Q}{T_j - T_c} \tag{2}$$

According to the similar characteristics of an electrical circuit, thermal resistance and thermal capacitance are introduced in a thermal circuit. The thermal model is fitted by nth order Foster or Cauer model. To obtain the thermal model, the temperature cooling curve is necessary, as shown in equation (3).

$$T_{jc\downarrow} = P \sum_{i=1}^{n} R_i e^{-\frac{-t}{R_i C_i}} \tag{3}$$

where $T_{jc\downarrow}$ is the junction temperature during the cooling stage, t is the time, and n is the order of the fitted Foster model.

As $Z_{jc} = T_{jc\uparrow}/P$, the transient thermal impedance curve is obtained by normalizing the temperature response curve with power, and it is shown in equation (4). $T_{jc\uparrow}$ is the temperature during the heating stage. It is not straightforward to characterize the temperature increasing stage due to the self-heating of the chip. Therefore, the temperature cooling stage is usually used that is when the high current is turned off and a small current is turned on. The temperature cooling stage is obtained by measuring the collector voltage and applying the K calibration coefficient.

$$Z_{jc} = \sum_{i=1}^{n} R_i (1 - e^{-\frac{-t}{R_i C_i}}) \tag{4}$$

The process for obtaining K calibration is as followed. the IGBT module was placed in a thermal chamber at a temperature of 40 °C for about 10 min. The first temperature and voltage points were obtained with a current of 0.1 A. The process was then repeated 3 times at temperatures of 55 °C, 70 °C, and 85 °C.

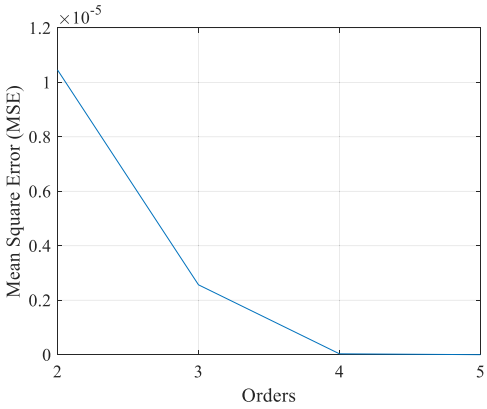

FIGURE 6. Mean square error of different-order model.

The model of MMG75SR120B (70 A/1200 V) IGBT modules is used to obtain the K calibration parameter, the result is expressed in Equation (5).

$$V_{ce} = -0.0021 T_j + 0.6082 \tag{5}$$

where V_{ce} is collector voltage, T_j is junction temperature.

After the K calibration was obtained, the measured voltage with a small current (0.1 A) was applied in the thermal cooling stage, then it was converted to an accurate junction temperature.

The junction-to-case thermal resistance was obtained by a transient dual interface method. The temperature in the cooling stage was measured twice with and without putting grease on the interface, and the separate point of these two cooling curves indicates the interface of the module and the heatsink, the cooling curve before that points is the temperature cooling curve of the module and after that point is the cooling curve of the heatsink. After the thermal cooling curve of the module is obtained, it is used for the thermal resistance and thermal capacitance estimation.

The Foster model is used to represent the thermal transfer process, multiple values of n in the Foster model ranging from $n = 2$ to $n = 5$ were used to fit the transient thermal process, the mean square error (MSE) of the regression fit is used for making the number-accuracy trade-off.

The MSE result of different orders of the Foster model is shown in Figure 6, number 4 is the elbow points of the MSE curve, therefore, the fourth-order Foster model was selected as the thermal simulation model. The result also shows that the Foster model represents the thermal response process accurately and MSE is less than 1.2×10^{-5} in transient process, therefore the simulation junction temperature is used to represent actual junction temperature.

Once $n = 4$ is finalized, the simulation data was compared with the other measurement data in the thermal cooling stage.

Figure 7 shows the thermal response curve of the junction-to-case temperature, it shows a strong agreement between the thermal simulation model and the measurement results in the transient process, where the fourth-order model was used in the transient junction temperature simulation.

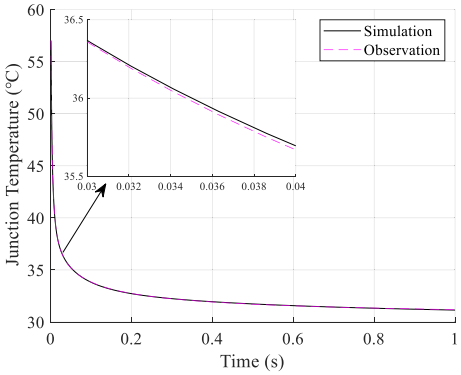

FIGURE 7. Fourth-order model simulation and measurement result.

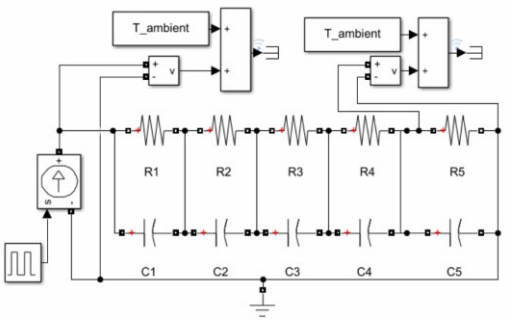

FIGURE 8. Equivalent thermal network simulation circuit diagram.

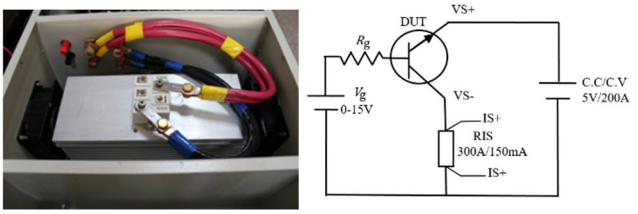

(a) (b)

FIGURE 9. Experiment setup and circuit diagram for IGBT module.

Figure 8 is a simulation schematic of a Foster model in MATLAB/Simulink. Four-order of the thermal model was adopted for junction-to-case temperature and another order was adopted for case-to-air temperature, thereafter, the gradient descent method was used to fit the thermal resistance R5 and heat capacitance C5 value.

To verify the validity of the case temperature results. An experimental case temperature data is compared with the simulated data. The measurement setup is shown in Figure 9, The IGBT module is installed in a chamber shown in Figure 9a and wired using the circuit diagram shown in Figure 9b. The measurements can be controlled from outside of the chamber using a control panel. The IGBT device under test (DUT), was powered by two supplies, a program-controlled test power supply of 5 V/200 A and a gate-foot program control power supply of 0–15 V. The gate pin series resistance of 10 Ω/2 W was used to limit the input current

TABLE 1. Thermal resistance and thermal capacitance results.

R1	R2	R3	R4	R5
0.19778	0.030003	0.03069	0.011484	1.2466
C1	C2	C3	C4	C5
0.232644	0.032697	0.297831	0.007715	195

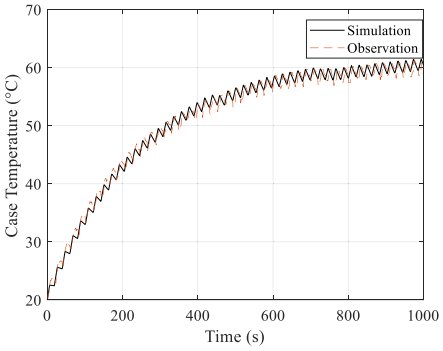

FIGURE 10. Simulation and experiment results of case temperature.

whereas a current transformer (RIS) of 150mA–300 A was used at the source terminal.

The case temperature was measured in working conditions with gate signal 20s per cycle at 50% duty, a current of 50 A, and a blocking voltage of 100 V. The comparison of the simulation data and measurement data is shown in Figure 10. In the transient process, the RMSE of simulation and measured data is 0.6 °C, the case temperature is accurately simulated in the transient process.

Table 1 shows the parameter values. R1 to R4 are the junction-to-case thermal resistances, and C1 to C4 are the junction-to-case thermal capacitances. R5 and C5 are the case-to-air thermal resistance and thermal capacitance.

Through the above theoretical analysis and simulation results of IGBT transient thermal response, it is found that the thermal response curve of IGBT junction temperature and case temperature is greatly affected by the timing parameters. Theoretically, the time series nonparametric model captures not only the relationship between the parameters but also the relationship between the thermal parameters at different times. It should have a good prediction effect for the parameters with delay characteristics such as thermal response. To verify the above theoretical analysis, a time series nonparametric model is constructed to observe the prediction effect of thermal response parameters of the time series nonparametric model under different thermal loads.

To acquire the training and testing data for the nonparametric model, the simulation model is used as it is powerful enough to represent the experimental data under varying conditions. It should be noted that to obtain the simulation model of the IGBT, the K calibration coefficient and accurate measurement of junction temperature in the cooling process are required. However, the nonparametric model only needs a period of real-time data to establish the model, and then the junction temperature and case temperature will be predicted at any given temperature and power.

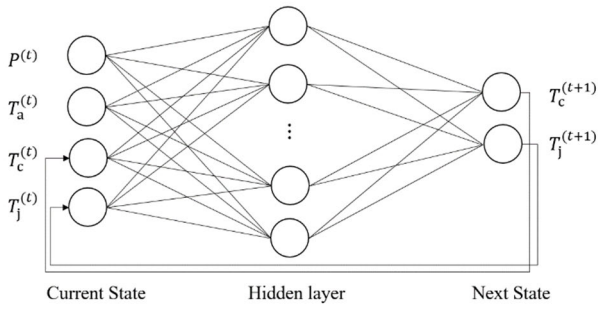

FIGURE 11. Time-series nonparametric model framework for IGBT.

IV. ESTABLISHMENT OF TIME-SERIES NONPARAMETRIC MODEL

The framework of the model for training and estimating data with time series attributes is shown in Figure 11. In the process of constructing the time series nonparametric model, the $P^{(t)}, T_a^{(t)}, T_c^{(t)}, T_j^{(t)}$ of the current time are sorted into a data block as input data, $T_j^{(t+1)}$ is sorted as the output data, the weight and bias between the parameters at the current time and those at the future time will be used for the subsequent junction temperature prediction. In the case of predicting the case temperature and junction temperature at the same time, $P^{(t)}, T_a^{(t)}, T_c^{(t)}, T_j^{(t)}$ at the current time are sorted into a data block and taken as the inputs of the model, $T_c^{(t+1)}, T_j^{(t+1)}$ are the outputs data block, they will be used to predict the subsequent junction and case temperature of the module.

To simplify the description, the input layer of neuro $P^{(t)}, T_a^{(t)}, T_c^{(t)}, T_j^{(t)}$ are represent by x_1, x_2, x_3, x_4 separately, the neurons in the middle layer are $a_n^{(p)}$, superscript p is the number of layers where neurons are located, and subscript n is the sequence number of neurons in this layer. The neurons in the output layer are $T_c^{(t+1)}(x)$ and $T_j^{(t+1)}(x)$. In the forward propagation, the calculation formula of each neuron is shown in equation (6).

$$a_n^{(2)} = g(\sum_{1}^{m} \theta_{i,j}^{(k)} x_j) \tag{6}$$

where $a_n^{(2)}$ is the second layer of number n neurons value, $\theta_{i,j}^{(k)}$ is weight from k layer to $k+1$ layer, subscript i represents the sequence number of $k+1$ neurons connected by the weight, subscript j represents the sequence number of the layer k neurons connected by the weight, The weight matrix can be expressed as $\boldsymbol{\theta}^{(k)}$, $g(x)$ is the activation function. If the number of neurons in layer k is s_j, the number of neurons in the $k+1$ layer is s_{j+1}, then the dimension of the weight matrix is $s_{j+1} \times (s_j + 1)$.

The calculation formulas of neurons in the output layer are shown in equations (7) and (8).

$$T_c(x) = a_1^{(3)} = g(\theta_{10}^{(2)} a_1^{(2)} + \theta_{11}^{(2)} a_2^{(2)} + \ldots + \theta_{1n}^{(2)} a_n^{(2)}) \tag{7}$$

$$T_j(x) = a_2^{(3)} = g(\theta_{20}^{(2)} a_1^{(2)} + \theta_{21}^{(2)} a_2^{(2)} + \ldots + \theta_{2n}^{(2)} a_n^{(2)}) \tag{8}$$

where n is the number of neurons in the hidden layer.

The error of each layer in backpropagation is shown in equations (9) and (10).

$$\delta_j^{(3)} = a_j^{(3)} - y_j \tag{9}$$

$$\boldsymbol{\delta}^{(2)} = (\boldsymbol{\theta}^{(2)})^{\mathrm{T}} \boldsymbol{\delta}^{(3)} \times g'(z^{(2)}) \tag{10}$$

where superscript of $\delta_j^{(k)}$ is the layer, subscript k is the sequence number of neurons in the layer. $a_j^{(3)}$ is the third layer of the neuron network, it is the last layer of the neural network $T_c(x)$ and $T_j(x)$. $\boldsymbol{\delta}^{(2)}$ is the slope matrix of the damage function in the second layer of the neural network at each neuron. $z^{(2)}$ is the intermediate variable that facilitates the calculation of the slope of the weight.

The updated weight is calculated, as shown in equation (11).

$$\Delta_{m,j}^{(k)}(u+1) = \Delta_{m,j}^{(k)}(u) + a_j^{(k)} \delta_m^{(k+1)} \tag{11}$$

where $\Delta_{i,j}^{(k)}(u+1)$ are updated parameters, $\Delta_{i,j}^{(k)}(u)$ are parameters before updated, $a_j^{(k)}$ is the learning rate, superscript k is the layer, subscript j is the order number of neurons in this layer, subscript m is the number of groups of input data.

The partial derivative of the loss function is obtained by equation (12).

$$\frac{\partial}{\partial \theta_{m,j}^{(k)}} J(\theta) = \frac{1}{m} \Delta_{m,j}^{(k)} + \lambda \theta_{i,j}^{(k)} \tag{12}$$

where $J(\theta)$ is the loss function.

In the follow-up prediction process, the established time series nonparametric model takes the measured power and ambient temperature of the module as the input, which can quickly predict the junction and case temperature of the module. Comparing with the traditional model, the time-series method takes the correlation between two adjacent states into account, it has good applicability for the prediction of thermal response value which has delay characteristics.

The framework construction and implementation of time series ANN are completed in MATLAB. The neurons of the hidden layer are set to 50 to make a time consumption-accuracy trade-off.

In the process of training, 70% of the data is used for training, 15% is used for validation, and 15% for testing. The Levenberg-Marquardt method is used to iterate 1000 times. The MSE of both the training, validation and test data decreases to less than $10e^{-4}$ after 1000 times.

Three groups of data are obtained by simulation, one for establishing the time-series nonparametric model and the other two (test data A and test data B) for testing the model under two different conditions. Each group of data records time-series data of junction temperature, case temperature, ambient temperature, and power of 3000 s.

As mentioned in Section III, the simulation model simulates time-series junction temperature and case temperature by real-time power and ambient temperature. These four parameters of time-series data obtained from simulation data

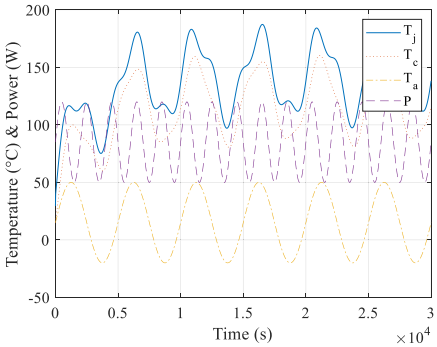

FIGURE 12. Junction and case temperature simulation results of the training data.

are used as ground truth for training and testing the time-series nonparametric model.

There are two cases in which the time-series nonparametric model is used. In the first case, the junction temperature is predicted when the case temperature is monitored. In the second case, the junction temperature and case temperature are predicted when the case temperature is not monitored. The details are introduced in the next two sections.

A. TEMPERATURE ESTIMATION CASE I

Recall that in case I, the junction temperature is predicted when the case temperature is known. In this case, the ambient temperature settings of the test data set A are: amplitude 35, bias 15, frequency 0.04pi, and phase 0. The power settings are amplitude 35, bias 85, frequency 0.01pi, and phase 0.

Figure 12 presents the data used to establish the time-series nonparametric model. The ambient temperature and power are given, and the junction temperature and case temperature are simulated by the simulation model.

In the process of training and testing, the initial input of the model has six parameters, which are power and the ambient temperature at the current moment, the power and the ambient temperature, the junction temperature, and the case temperature at the previous moment. The output is the current junction temperature. The predicted junction temperature will be used as the input parameter to calculate the junction temperature for the next moment.

To showcase the generalization of the method, the other two groups (test data set A and test data set B) in completely different states are used for testing. The ambient temperature and power settings of the test data are different. The ambient temperature settings of the test data set A are: amplitude 35, bias 15, frequency 0.04pi, and phase 5. The power settings are amplitude 35, bias 85, frequency 0.01pi, and phase 7. The time-series data is shown in Figure 13.

The junction temperature results of the test data set A are shown in Figure 14. The RMSE of simulation results and predicted results is 0.28 °C.

The ambient temperature settings of the test data set B are amplitude 30, bias 15, frequency 0.001pi, and phase 7. The power settings are amplitude 33, bias 85, frequency 0.03pi, and phase 3. The time-series data are shown in Figure 15.

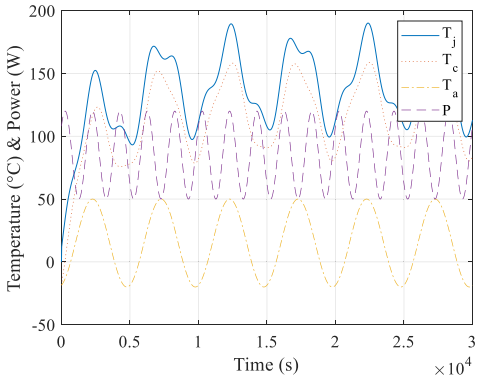

FIGURE 13. Junction and case temperature simulation results of test data A.

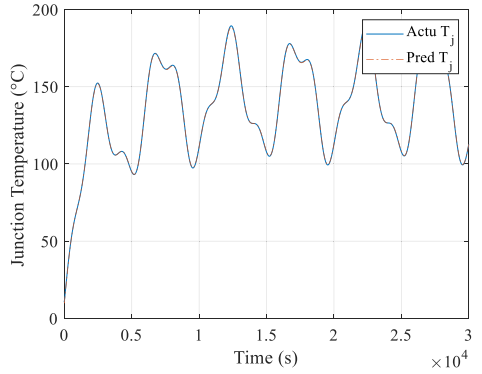

FIGURE 14. Junction temperature prediction result of the time-series nonparametric model for test A.

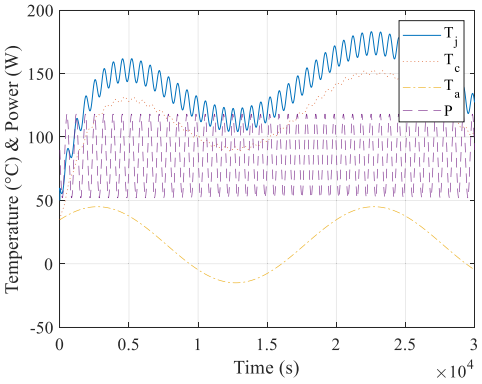

FIGURE 15. Junction and case temperature simulation results of test data B.

Figure 16 shows the time-series nonparametric model predicted junction temperature comparing with simulation results The RMSE of simulation results and predicted results is 0.22 °C.

When the ambient temperature, power, and case temperature are continuously monitored, the process of junction temperature prediction is effectively verified by the time-series nonparametric model. It indicates that the time-series nonparametric model is a very useful method for online junction prediction when the case temperature is monitored. However, the case temperature cannot be monitored online

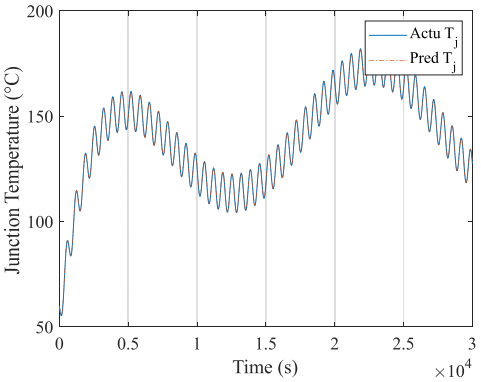

FIGURE 16. Junction temperature prediction results of the time-series nonparametric model for test B.

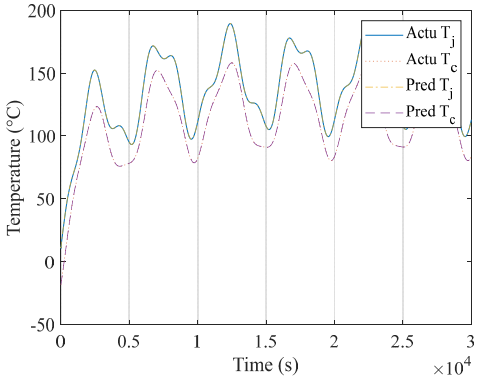

FIGURE 17. Junction and case temperature prediction results of the time-series nonparametric model (500 neurons) for test A.

for some cases, it is necessary to test whether the junction temperature and case temperature can be predicted accurately when the case temperature is not monitored.

B. TEMPERATURE ESTIMATION CASE II

In this section, the time-series nonparametric model is used to predict the junction temperature and case temperature in real-time, when the case temperature cannot be monitored.

In the process of training and testing, the same six parameters were used which are power and the ambient temperature at the current moment, the power, the ambient temperature, the junction temperature, and the case temperature at the previous moment. The output is the junction temperature and the case temperature at the current moment.

The 50 neurons time-series nonparametric model was tried at first, the RMSE of the time-series nonparametric predicted model and simulation model is as high as 1 °C. To improve the prediction accuracy, the number of neurons was increased to 500. The junction temperature and case temperature of test data set A obtained are shown in Figure 17. The RMSEs of the simulation and predicted results for the junction temperature and case temperature are 0.11 °C and 0.11 °C, respectively.

The predictions of the junction temperature and case temperature of test data set B are shown in Figure 18. The RMSEs of simulation results and predicted results for

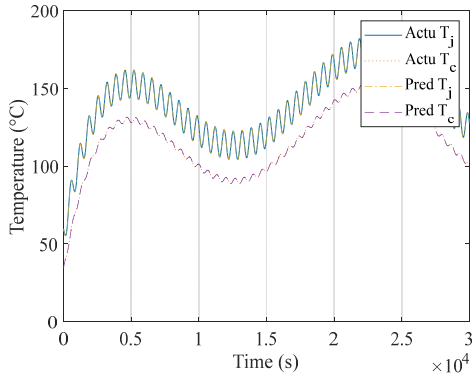

FIGURE 18. Junction and case temperature prediction results of the time-series nonparametric model (500 neurons) for test B.

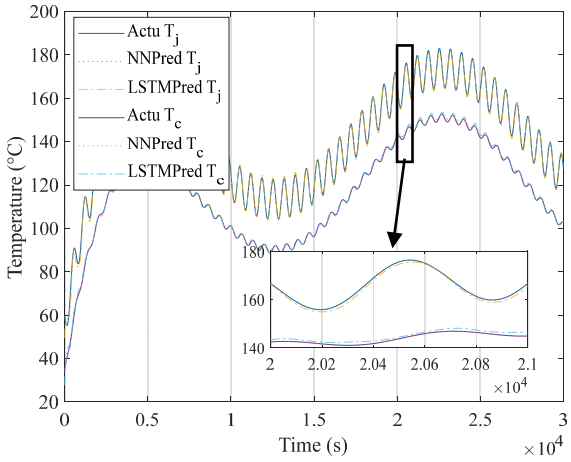

FIGURE 19. Comparison of the time-series ANN predicted results and LSTM predicted results with actual results.

junction temperature and case temperature are 0.10 °C and 0.09 °C respectively.

It is evident that for the model with 500 neurons, the junction temperature prediction accuracy in the transient process is high. It indicates that the time-series nonparametric model is accurate for online junction temperature. Besides, the process of establishing the time-series nonparametric model is simpler than that of the simulation model. The time-series nonparametric model is established only by using a segment of real-time state data.

The comparison results of time-series ANN and LSTM are shown in Figure 19. The RMSEs of time-series ANN predicted result and LSTM predicted result with actual junction temperature are separately 0.3 °C and 0.4 °C.

In the above analysis, the simulation data are used to analyze the prediction results of the time series nonparametric model and verify the results effectively. To further verify the prediction accuracy of the time series nonparametric model for predicting the experimental result, the experimental data of case temperature in transient process and prediction data of time series nonparametric model are selected for comparison. The comparison results are shown in Figure 20. It shows that the RMSE result of the time series nonparametric model and

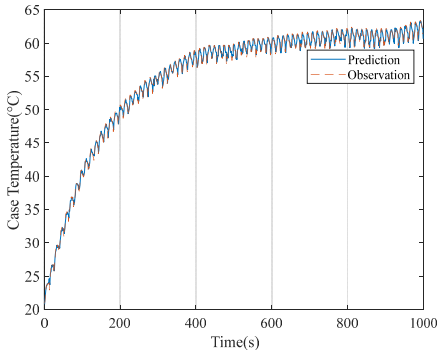

FIGURE 20. Comparison between the experimental results and the prediction results of time series nonparametric mode.

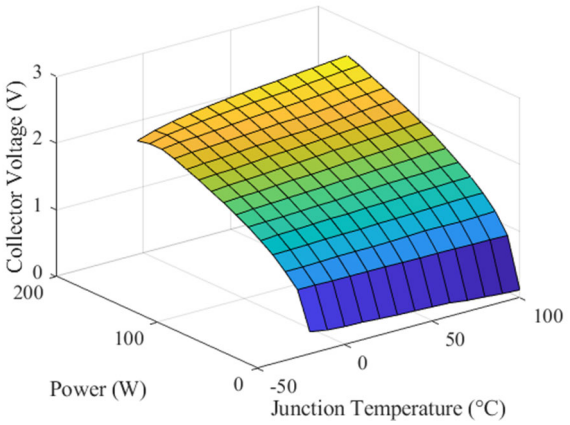

FIGURE 21. The relationship of junction temperature, collector voltage, and power.

the experimental data is 0.4 °C, which indicates that the time series nonparametric model has high accuracy in predicting the transient case temperature of the module. Comparing with the data in Figure 10 when using the simulation model to estimate case temperature, the RMSE of time-series nonparametric model result to experimental result is 0. 2°C smaller.

In all, supposing that the thermal response is a Foster likely model which is theoretically accepted, the time-series nonparametric model is proven that it captures the relationship of different parameters in different timing and the RMSE of Foster model and time-series nonparametric model predicted result is less than 0.3 °C. Supposing that all the model error and system error are considered, the experimental data is used to obtain both simulation model and non-parametric model, the RMSE of simulation result to experimental result is 0.6 °C, and RMSE of time-series nonparametric model is 0.4 °C, which shows that the time-series nonparametric model works better than the traditional thermal model. The time series nonparametric model has higher predicting accuracy than the traditional thermal model for the thermal response curve prediction which has delay characteristics, and its robustness of this method is proved by the theoretical analysis of thermal characteristics and its applicability to different scenarios.

The junction temperature changes very fast in the dynamic process. It is generally accepted that measuring it directly with high accuracy in the dynamic process is very hard. The equivalent thermal network model obtained by the transient double interface method is the optimal prediction method when the case temperature is known. The MSE of the fourth-order Foster thermal model for the description of the transient thermal response curve is less than 1.2×10^{-5}. Its ability for describing the dynamic process has been verified by theory and experiment, so the simulated junction temperature is used as the equivalent measured junction temperature. Time-series nonparametric model has been discussed above to show its accuracy for predicting the junction temperature.

Noted that the paper focus on condition monitoring the chip solder layer only, the different thermal characteristic caused by bond wire degradation is not considered in the paper and should be further explored.

V. NONPARAMETRIC MODEL AND STATE-OF-HEALTH ESTIMATION PROGNOSTIC

In this section, the nonparametric model is used to predict the junction temperature and case temperature of the module in real-time without considering the module degradation. The results above prove that the RMSE results of the predicted junction temperature and case temperature have strong agreement with the actual measurement results of the module. Therefore, the accurately predicted junction temperature and case temperature of the module in the healthy state are obtained by using the time series nonparametric model when given the power and ambient temperature.

The difference between the estimated value and the measured value is used to estimate the state-of-health as shown in Figure 4, that is because the estimated value is equivalent to the time-series data before the module aged, while the measured value is the real-time value after the module degraded

In the actual operation of IGBT, the collector voltage can be measured in real-time, and the measurement accuracy is high. Therefore, the interdependence of junction temperature, collector voltage, and collector current is established through the experimental data, then the relationship can be transferred to the relationship of junction temperature, collector voltage, and power. The nonparametric model is used for collector voltage prediction by junction temperature and collector current, it is used to replace the look-up table. Thereafter, the real-time collector voltage is estimated by the junction temperature and current through the second nonparametric model. The junction temperature is measured by the thermocouple attaching method, the IGBT package is perforated from the side, and the thermocouple is in direct contact with the IGBT module chip. The relationship between junction temperature, collector voltage, and power is shown in Figure 21. Thereafter, the second nonparametric model is finalized and the real-time collector voltage value is obtained by giving the real-time junction temperature and current.

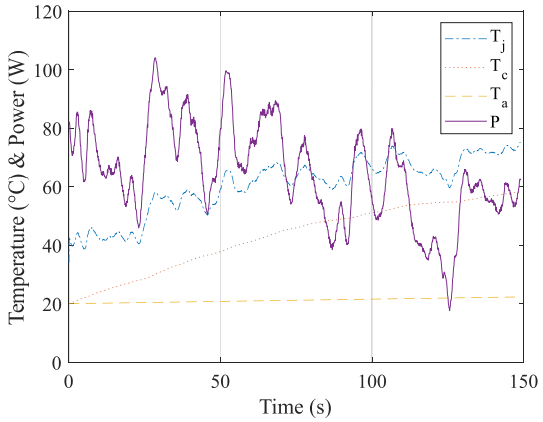

FIGURE 22. Simulated junction temperature and case temperature by ambient temperature and power.

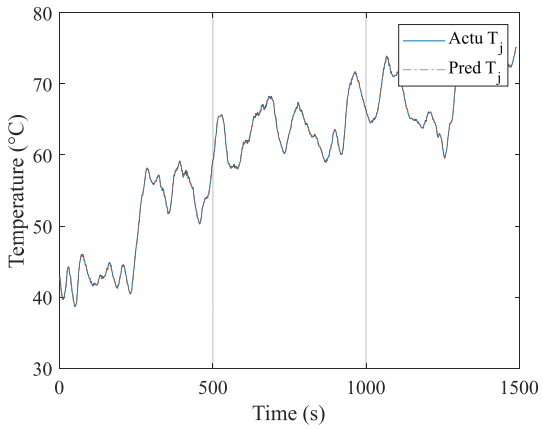

FIGURE 23. Nonparametric model predicated junction and case temperatures of IGB.

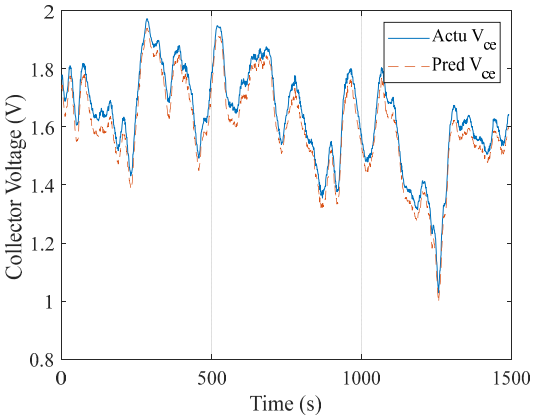

FIGURE 24. The predicted and simulated collector voltage of real-time dataset one.

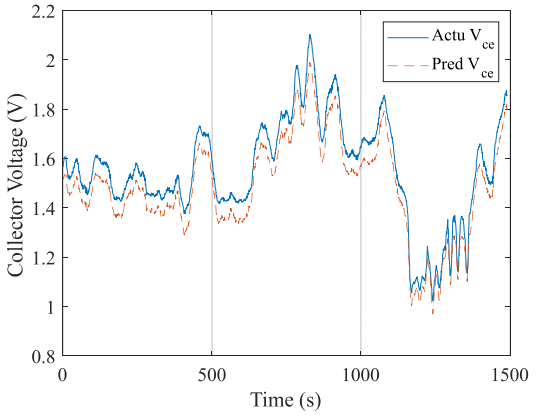

FIGURE 25. The predicted and simulated collector voltage of real-time dataset two.

The real-time power and ambient temperature and simulated junction temperature and case temperature are shown in Figure 22.

The junction temperature predicted by the nonparametric model is shown in Figure 23, when power, ambient temperature, and case temperature are given. The RMSE between the predicted value by the nonparametric model and simulation system is 0.05 °C. It indicates that the nonparametric model has the same effect as the simulation model for the prediction of in-service junction temperature.

Once the junction temperature has been estimated, the real-time collector voltage is obtained using the nonparametric model. The result is compared with the measured collector voltage and the result is shown in Figure 24.

In Figure 24, the solid line is the measured collector voltage value, that is, the real-time voltage value of the module and the dotted line is the collector voltage predicted by the nonparametric model under the healthy state.

The state of health of IGBT is the condition of a module compared to its ideal conditions, it is estimated by. parameter average percentage deviation and the units of state-of-health is percent points. A module's state of health is assumed to be 100% at the time of manufacture and will decrease over time and use. The module state-of-health is determined by monitoring the average percentage deviation in collector voltage value from the expected voltage. The formula for the voltage percentage deviation is shown in Equation (13).

$$P = \frac{1}{n}\sum_{i=1}^{n}\frac{V_{\mathrm{d}}(i) - V_{\mathrm{h}}(i)}{V_{\mathrm{h}}(i)} \tag{13}$$

where V_{d} is the measured real-time voltage value, V_{h} is the real-time voltage value predicted by the nonparametric model, n is the number of data points. The average percentage deviation of these 1500 points is 2.56%.

After another period of aging, the second real-time data is measured, the result of the measured collector voltage and predicted collector voltage is shown in Figure 25, the average percentage deviation of these 1500 points is 3.02%. And the module stopped working after less than 10 hours.

By analyzing the data of eight aging modules, it is found that the voltage increment of the module is 3.01%, 2.92%, 3.12%, 3.23%, 2.81%, 3.28%, 3.20%, and 3.18% respectively before the catastrophic failure. The 99.5% lower limit of the one-sided confidence interval of the voltage increment percentage is calculated. For $\forall\theta\epsilon\Theta$, when the inequality $\mathrm{P}\{\theta > \theta_1\} \geq 1 - \alpha$ is satisfied, the one-sided confidence

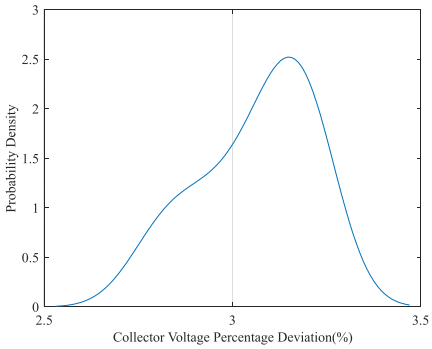

FIGURE 26. The probability density function of voltage increment percentage.

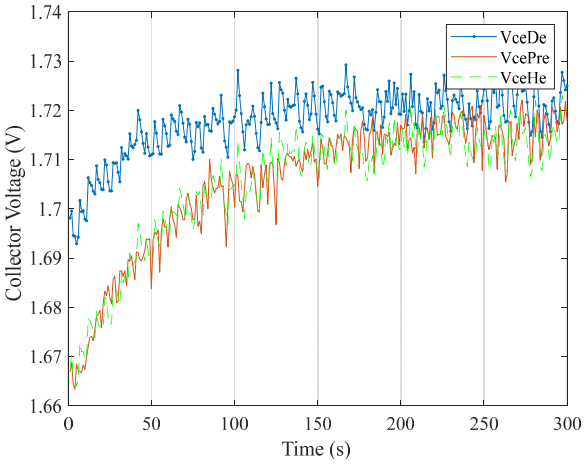

FIGURE 27. Experimental and predicted collector voltage before and after agin.

interval of $1-\alpha$ is (θ_1, ∞), and the one-sided lower confidence limit is θ_1.

For a normal distribution population with unknown mean and variance, the formula is $\frac{\bar{X}-\mu}{S/\sqrt{n}} \sim t_\alpha(n-1)$, the lower limit of the one-sided confidence interval of the module is obtained as $\bar{X} - \frac{S}{\sqrt{n}}t_\alpha(n-1)$, the probability distribution density function of the module is obtained as shown in Figure 26. The lower limit of one-sided confidence interval with 99.5% confidence interval is 3.09%.

When the voltage value increases by 3.09%, the module has a 99.5% probability of catastrophic failure. Therefore, when the equivalent voltage data of the module increases by 3.09%, the cumulative damage of the corresponding module is 1.

To further verify the method, experimental data are used to do the comparison with the predicted data. The power, ambient temperature, and collector voltage of a mission profile before the module experience catastrophic failure were collected. Then, the collector voltage in the health state was deduced in that specific mission profile by the collected data of power and ambient temperature. Because the predicted data indicates the collector voltage when the module was in a healthy state. and the data of the same mission profile before the module aged were compared with it and the results of predicted collector voltage and measured ones are shown in Figure 27. It shows that the predicted collector voltage is in good fit with that of the measured healthy state data. While the on and off time in the mission profile is set, the power and ambient temperature collected before and after aging have errors within 1 W and 1 °C. The predicted collector voltage tracked in trend with the measured data after aging and it is in good fit with measured data before aging, which indicates the effectiveness of the method. After verifying the effectiveness of the method, the measured collector voltage value before failure and predicted collector voltage are compared and the percentage voltage deviation increases by 3.11%. It can be seen from the figure that the aging state of the module can be predicted by the difference between the predicted collector voltage and the measured collector voltage under a certain mission profile.

VI. CONCLUSION

This paper proposes a time series non-parametric model method for time series data prediction. The method captures the relative relationship of time series features of multi-dimensional feature parameters by directly inputting the time series data which is collected in the complex working condition. The method solves the personalized parameter prediction and real-time parameter prediction problem, and the state-of-health of the module is evaluated based on the real-time parameter prediction. In the approach a time-series nonparametric model of the IGBT module is proposed and constructed, the measured power and ambient temperature data are used to deduce the health state data junction and case temperature, and the difference between the monitoring junction temperature or case temperature data is compared with the predicted data to judge the real-time health state of the module. Compared with traditional methods, the time series non-parametric model method is good for implementation, it not only saves characteristic experiments but also the process of mathematical model induction and time series state equation derivation.

The method proposed in this paper has good expansibility. Because the data measurement method applied to training is simple, the time series data of each parameter of the module in the health state is collected before the module is packaged, and the data is stored as the personalized health data of the module. It then provides the basis for the later real-time junction temperature prediction and state-of-health evaluation easily. Compared with the traditional method of uniform parameters of the equivalent thermal model, this method considers personalized differences of modules and provides a new method for health assessment of modules under different mission profiles, which has high practical value for modules with long service time.

REFERENCES

[1] U.-M. Choi and F. Blaabjerg, "Separation of wear-out failure modes of IGBT modules in grid-connected inverter systems," *IEEE Trans. Power Electron.*, vol. 33, no. 7, pp. 6217–6223, Jul. 2018, doi: 10.1109/TPEL.2017.2750328.

[2] J. L. Hudgins, "Power electronic devices in the future," *IEEE J. Emerg. Sel. Topics Power Electron.*, vol. 1, no. 1, pp. 11–17, Mar. 2013, doi: 10.1109/JESTPE.2013.2260594.
[3] A. Benmansour, S. Azzopardi, J. C. Martin, and E. Woirgard, "A step by step methodology to analyze the IGBT failure mechanisms under short circuit and turn-off inductive conditions using 2D physically based device simulation," *Microelectron. Rel.*, vol. 47, nos. 9–11, pp. 1800–1805, Sep. 2007.
[4] M. H. M. Sathik, J. Pou, S. Prasanth, V. Muthu, R. Simanjorang, and A. K. Gupta, "Comparison of IGBT junction temperature measurement and estimation methods-A review," in *Proc. Asian Conf. Energy, Power Transp. Electrific. (ACEPT)*, Oct. 2017, pp. 1–8, doi: 10.1109/ACEPT.2017.8168600.
[5] L. Dupont, Y. Avenas, and P.-O. Jeannin, "Comparison of junction temperature evaluations in a power IGBT module using an IR camera and three thermosensitive electrical parameters," *IEEE Trans. Ind. Appl.*, vol. 49, no. 4, pp. 1599–1608, Jul. 2013, doi: 10.1109/TIA.2013.2255852.
[6] M. Piton, B. Chauchat, and J. F. Servière, "Implementation of direct Chip junction temperature measurement in high power IGBT module in operation—Railway traction converter," *Microelectron. Rel.*, vols. 88–90, pp. 1305–1310, Sep. 2018, doi: 10.1016/j.microrel.2018.06.114.
[7] Y. Yuan, D. Xiang, and C. Ning, "Self-calibration for IGBT junction temperature measurement in power converter," in *Proc. IEEE 8th Int. Power Electron. Motion Control Conf. (IPEMC-ECCE Asia)*, May 2016, pp. 3125–3130, doi: 10.1109/IPEMC.2016.7512795.
[8] J. Zhang, M. Du, L. Jing, K. Wei, and W. G. Hurley, "IGBT junction temperature measurements: Inclusive of dynamic thermal parameters," *IEEE Trans. Device Mater. Rel.*, vol. 19, no. 2, pp. 333–340, Jun. 2019, doi: 10.1109/TDMR.2019.2910182.
[9] M. A. Eleffendi and C. M. Johnson, "Application of Kalman filter to estimate junction temperature in IGBT power modules," *IEEE Trans. Power Electron.*, vol. 31, no. 2, pp. 1576–1587, Feb. 2016, doi: 10.1109/TPEL.2015.2418711.
[10] M. Ouhab, Z. Khatir, A. Ibrahim, J.-P. Ousten, R. Mitova, and M.-X. Wang, "New analytical model for real-time junction temperature estimation of multichip power module used in a motor drive," *IEEE Trans. Power Electron.*, vol. 33, no. 6, pp. 5292–5301, Jun. 2018, doi: 10.1109/TPEL.2017.2736534.
[11] Y. Hu, P. Shi, H. Li, and C. Yang, "Health condition assessment of base-plate solder for multi-chip IGBT module in wind power converter," *IEEE Access*, vol. 7, pp. 72134–72142, 2019, doi: 10.1109/ACCESS.2019.2918029.
[12] R. Quan, H. Li, Y. Hu, and P. Gao, "A novel IGBT health evaluation method based on multi-label classification," *IEEE Access*, vol. 7, pp. 47294–47302, 2019, doi: 10.1109/ACCESS.2019.2909741.
[13] M. Ma, B. Ji, J. Han, J. Wang, M. Zhan, and N. Xiang, "*In-situ* health monitoring of IGBT modules of an on-line medium-voltage inverter system using industrial Internet of Things," *CSEE J. Power Energy Syst.*, vol. 6, no. 3, pp. 638–648, Sep. 2020, doi: 10.17775/CSEEJPES.2019.01670.
[14] Y. Zhang, Y. Liu, C. Li, and J. Li, "Analysis of fault precursor parameters under accelerated aging tests for IGBT modules," in *Proc. 17th China Int. Forum Solid State Lighting Int. Forum Wide Bandgap Semiconductors China (SSLChina: IFWS)*, Nov. 2020, pp. 238–241, doi: 10.1109/SSLChinaIFWS51786.2020.9308699.
[15] Y. Yang, Q. Zhang, and P. Zhang, "A fast IGBT junction temperature estimation approach based on ON-state voltage drop," *IEEE Trans. Ind. Appl.*, vol. 57, no. 1, pp. 685–693, Jan. 2021, doi: 10.1109/TIA.2020.3030753.
[16] N. Patil, D. Das, and M. Pecht, "A prognostic approach for non-punch through and field stop IGBTs," *Microelectron. Rel.*, vol. 52, no. 3, pp. 482–488, Mar. 2012, doi: 10.1016/j.microrel.2011.10.017.
[17] X. Ye, C. Chen, Y. Wang, G. Zhai, and G. J. Vachtsevanos, "Online condition monitoring of power MOSFET gate oxide degradation based on miller platform voltage," *IEEE Trans. Power Electron.*, vol. 32, no. 6, pp. 4776–4784, Jun. 2017, doi: 10.1109/TPEL.2016.2602323.
[18] Y. Zhang, R. Xiong, H. He, and Z. Liu, "A LSTM-RNN method for the lithuim-ion battery remaining useful life prediction," in *Proc. Prognostics Syst. Health Manage. Conf. (PHM-Harbin)*, Jul. 2017, pp. 7–10, doi: 10.1109/PHM.2017.8079316.
[19] H. Zhao, H. Liu, W. Hu, and X. Yan, "Anomaly detection and fault analysis of wind turbine components based on deep learning network," *Renew. Energy*, vol. 127, pp. 825–834, Nov. 2018, doi: 10.1016/j.renene.2018.05.024.
[20] G. Netam and A. Yadav, "Fault detection, classification and section identification on distribution network with D-STATCOM using ANN," *Int. J. Adv. Technol. Eng. Explor.*, vol. 3, no. 23, pp. 150–157, Nov. 2016, doi: 10.19101/ijatee.2016.323001.
[21] X. Zeng, Z. Li, W. Gao, M. Ren, J. Zhang, Z. Li, and B. Zhang, "A novel virtual sensing with artificial neural network and K-Means clustering for IGBT current measuring," *IEEE Trans. Ind. Electron.*, vol. 65, no. 9, pp. 7343–7352, Sep. 2018, doi: 10.1109/TIE.2018.2793196.
[22] T. Dragicevic, P. Wheeler, and F. Blaabjerg, "Artificial intelligence aided automated design for reliability of power electronic systems," *IEEE Trans. Power Electron.*, vol. 34, no. 8, pp. 7161–7171, Aug. 2019, doi: 10.1109/TPEL.2018.2883947.

XIANGXIANG LIU was born in Hebei, China, in 1991. She received the B.S. and M.S. degrees in electrical engineering from the Hebei University of Technology, Tianjin, China, in 2013 and 2016, respectively, where she is currently pursuing the Ph.D. degree in electrical engineering. From 2017 to 2019, she was a Visiting Student with the Center for Advanced Life Cycle Engineering (CALCE), University of Maryland, USA. Her main research interests include online monitoring and anomaly detection of semiconductor, prognostic, and health management of the power systems.

TIANLEI JIAO was born in Hebei, China, in 1990. He received the B.S. degree in electrical engineering from the Hebei University of Technology, Tianjin, China, in 2013. He is currently a Data Engineer with Beiyang Hongyun (Tianjin) Cyber Technology Ltd., Tianjin. His position is the Technical Director. His main research interests include data mining, application of artificial intelligence in various fields, prognostic and health management of power systems.

DIGANTA DAS (Member, IEEE) received the B.Tech. degree in manufacturing science and engineering from the Indian Institute of Technology, Kharagpur, India, and the Ph.D. degree in mechanical engineering from the University of Maryland, College Park, MD, USA. He is currently a Member of the Research Staff at the Center for Advanced Life Cycle Engineering (CALCE), University of Maryland. His expertise is in reliability, environmental, and operational ratings of electronic parts; uprating; electronic part reprocessing; counterfeit electronics; technology trends in the electronic parts and parts selection; and management methodologies. He performs benchmarking processes and organizations of electronics companies for parts selection and management and reliability practices. He has published more than 60 articles on these subjects and presented his research at international conferences and workshops. His current research interests include counterfeit electronics avoidance and detection, light-emitting-diode failure mechanisms, cooling systems in telecommunications infrastructure and their impact on reliability, and power electronics reliability. He is a member of IMAPS and SMTA. He is an Editorial Board Member for the journal *Microelectronics Reliability* and *Circuit World*. He is currently the Vice Chair of the standards group of the IEEE Reliability Society. He had been the Technical Editor for two IEEE standards. He leads the Educational Outreach of CALCE with responsibility to develop interorganizational agreements on joint educational programs, training and internship program, and professional development. He is a Six Sigma Black Belt.

IJAZ HAIDER NAQVI (Member, IEEE) received the B.Sc. degree in electrical engineering from the University of Engineering and Technology Lahore, Pakistan, in 2003, the master's degree in radio communications from SUPELEC Paris, France, in 2006, and the Ph.D. degree in electronics and telecommunications from IETR-INSA Rennes, France, in 2009. He is currently an Associate Professor with the School of Science and Engineering, Lahore University of Management Sciences (LUMS), Pakistan. He has got several years of research experience in the wireless communications and wireless sensor networks. He also works in the area of reliability engineering investigating degradation and ageing of electronics specially Li-ion batteries. He has published several refereed articles in international journals and peer-reviewed international conference papers. His current research interests include 5G networks and beyond including system level aspects in wireless networks, millimeter wave wireless systems for 5G and 6G telecommunication and multi-antenna radar systems for civilian applications.

MICHAEL PECHT (Life Fellow, IEEE) received the B.S. degree in physics, the M.S. degree in electrical engineering, and the M.S. and Ph.D. degrees in engineering mechanics from the University of Wisconsin at Madison. He is a World-Renowned Expert in strategic planning, design, test, and risk assessment of information systems. He is currently a Professional Engineer. He is also a Chair Professor of mechanical engineering and a Professor of applied mathematics with the University of Maryland. He has also served on three NAS studies, two U.S. Congressional investigations in automotive safety, and as an Expert for the FDA. He is the Founder and the Director of the Center for Advanced Life Cycle Engineering, University of Maryland, which is funded by over 150 of the world's leading electronics companies at over U.S. 6 M/year. He is a Fellow of ASME, SAE, and IMAPS. He is the Editor-in-Chief of the IEEE Access. He was a recipient of the Highest Reliability Honor, the IEEE Reliability Society's Lifetime Achievement Award, in 2008. He received the NSF Innovation Award, in 2009, the National Defense Industries Association Award, the University of Wisconsin-Madison's College of Engineering Distinguished Achievement Award, in 2013, the University of Maryland's Innovation Award for his new concepts in risk management, in 2011, and the IEEE Exceptional Technical Achievement Award for his innovations in the area of prognostics and systems health management, in 2010. He received the IEEE Components, Packaging, and Manufacturing Award for Visionary Leadership in the development of physics-of-failure-based and prognostics-based approaches to electronic packaging reliability, in 2015. He received the Distinguished Chinese Academy of Sciences President's International Fellowship. He served as a Chief Editor of the IEEE Transactions on Reliability for a period of nine years and the *Microelectronics Reliability* for a period of 16 years.